J. Phys. B: At. Mol. Opt. Phys. **29** (1996) 1007–1023. Printed in the UK

Channel mixing in 4fng autoionizing series of barium

R van Leeuwen†, M Aymar‡, W Ubachs† and W Hogervorst†

† Laser Centre Vrije Universiteit, Department of Physics and Astronomy, De Boelelaan 1081, 1081 HV Amsterdam, The Netherlands

‡ Laboratoire Aimé Cotton§, CNRS II, Batiment 505, 91405 Orsay Cedex, France

Received 3 August 1995, in final form 27 November 1995

Abstract. Autoionizing 4fng $J = 0$–3 levels of barium in the energy range 88 240–90 460 cm^{-1} have been studied, both experimentally and theoretically. Excitation spectra, recorded in a three-step pulsed laser experiment based on an isolated-core excitation scheme, are confronted with eigenchannel R-matrix calculations. Series converging to the upper $4f_{7/2}$ and lower $4f_{5/2}$ thresholds are found to interact strongly, in particular for $J = 1$. As a result the observed 4fng resonances vary widely in width, shape and intensity. Although the complete R-matrix calculations involve many interacting channels for each J (up to 49 for $J = 3$), good agreement is found between experiment and theory and all observed resonances can be unambiguously assigned.

1. Introduction

In recent years sequential laser excitation following isolated-core excitation (ICE) schemes (Cooke and Gallagher 1978) has facilitated the selective probing of high-lying doubly excited states of the heavier alkaline-earth atoms. The ICE method has proven to be of value in the study of the effects of electron correlations in two-electron systems (Camus *et al* 1989, Jones and Gallagher 1990, Eichmann *et al* 1990). Effects of correlations between the valence electrons are, however, in many cases obscured by the influence of the extended 2^+ core of the alkaline-earth atoms. These core effects are small when both valence electrons are excited to a high-ℓ state ($\ell \geqslant 4$ for Ba) since the centrifugal barrier effect will then prevent the electrons from penetrating the 2^+ core. Doubly excited 4fng autoionizing levels of barium may serve as intermediate states in an excitation process to Ngng states with two non-core penetrating valence electrons. Detailed knowledge of the intermediate 4fng levels will be of importance to explain such observations. Previously Jones *et al* (1991) experimentally investigated the autoionizing $4f_{5/2}n$g $J = 3$ levels of Ba. In their experiment attention focused on levels located below the $6d_{5/2}$ threshold, in particular, on the double-circular 4f5g states. Recently, the experimental results were successfully analysed by Aymar and Luc-Koenig (1995) within the framework of the eigenchannel R-matrix method in combination with multichannel quantum defect theory (MQDT) (Aymar 1990, Greene and Aymar 1991 and references therein). The analysis of the 4f5g states showed the importance of electron correlation effects on autoionization widths. The eigenchannel R-matrix method has also been demonstrated to be of great value in the interpretation of even parity 4fnf states (Luc-Koenig *et al* 1994) as observed by de Graaff *et al* (1992) and of 4f7h states (van Leeuwen *et al* 1995).

§ The laboratoire Aimé Cotton is associated with the Université Paris-Sud, France.

0953-4075/96/051007+17$19.50

In this paper we present an experimental and theoretical investigation of 4fng autoionizing levels of Ba ($n \geqslant 7$) above the $6d_{5/2}$ threshold (88 189.79 cm^{-1} above the $6s^2$ ground state). The 4fng Rydberg series converge to the $4f_j$ ionization limits at 90 518.19 cm^{-1} for $j = \frac{7}{2}$ and 90 293.49 cm^{-1} for $j = \frac{5}{2}$. Three pulsed dye lasers were employed to populate 4fng levels in an ICE scheme. The 4fn'g $J' = 0$–3 levels were excited via $5d_{5/2}n$g $J = 1, 2$ intermediate levels ($n = 7$–26). The experimental results are compared with eigenchannel R-matrix calculations.

2. Experiment

The 4fng autoionizing states of barium were excited in an atomic beam in a three-step pulsed laser experiment. The experimental set-up was similar to the one used previously for the two-step excitation of 4f7h levels (van Leeuwen *et al* 1995). An atomic beam was produced by heating a tantalum oven containing a sample of Ba using a tungsten filament. During parts of the experiment a low voltage discharge was maintained between the heating filament and the oven to populate metastable 6s5d states. The atomic beam was perpendicularly intersected by linearly polarized laser light from three tunable dye lasers of 5 ns pulse duration, simultaneously pumped by the second or third harmonic output of a Nd:YAG laser. The excitation scheme is shown in the simplified energy level diagram of figure 1. Autoionizing 4fn'g states in the energy range 88 240–90 460 cm^{-1} were excited from low-lying autoionizing 5dng intermediate levels, which were excited either from the $6s^2\ {}^1S_0$ ground state via the 5d6p $^1P_1$ level at 28 554.19 cm^{-1} (path I), or from the metastable 6s5d $^3D_2$ state via the 5d6p $^3P_1$ level at 25 704.08 cm^{-1} (path II). As shown by van Leeuwen *et al* (1994) the intermediate 5dng levels are well described in a jK-coupling scheme, K resulting from the coupling of the total angular momentum j of the inner 5d electron with the orbital angular momentum ℓ of the outer ng electron. In the present experiment $5d_{5/2}n$g[3/2] $J = 1, 2$ and $5d_{5/2}n$g[5/2] $J = 2$ levels with $n = 7$–26 were used as intermediate states. The resolution in the experiment was sufficient to individually excite the $K = \frac{3}{2}$ and $K = \frac{5}{2}$ level since the bandwidth of the second dye laser (2 GHz) was smaller than the energy splitting between both levels for all n. The two J-components in the $K = 3/2$ doublet could, however, not be resolved. The $5d_{5/2}n$g states, which can be excited from 5d6p levels due to mixing of 5d6p and 5d4f wavefunctions, have low autoionization rates, e.g. for the $5d_{5/2}$5g[5/2] $J = 2$ level a width of 320 MHz, corresponding to a lifetime of 2 ns was reported (Luc-Koenig *et al* 1995). This allows for further excitation of a significant fraction of the atoms to $4f_j n$g[K']J' states by the frequency doubled output of a third dye laser (bandwidth 2 GHz) at wavelengths close to the $5d_{5/2} \rightarrow 4f_{7/2}$ ionic transition.

The 4fng levels, located at ~ 6 eV above the 6s ionization threshold, may autoionize into several continua. As a result Ba^+ ions in $6s_{1/2}$, $5d_j$, $6p_j$, $7s_{1/2}$, $6d_j$ states and, at energies above the $4f_{5/2}$ threshold, in $4f_{5/2}$ states can be produced. The energy of the UV photons driving the 5dng $\rightarrow$ 4fn'g transition is sufficient to photoionize Ba^+ $6d_j$, $7s_{1/2}$ and $4f_{5/2}$ ions. The resulting Ba^{++} ions were detected by an electron multiplier. This detection method differs from a scheme where fast electrons are detected to discriminate between autoionization products of intermediate and final states, as applied by Jones *et al* (1991) for 4f5g states. The 4f5g states are located below the $6d_j$ thresholds and decay mainly into 5d$\epsilon\ell$ continua, thus producing fast electrons (Aymar and Luc-Koenig 1995). The $4f_{7/2}n$g levels with $n \geqslant 7$, located above the $6d_j$ thresholds, are expected to decay predominantly into 6d$\epsilon\ell$ continua which results in the production of slow electrons (< 0.3 eV). The intermediate 5dng states produce slow electrons as well (< 0.7 eV) which are difficult to separate from

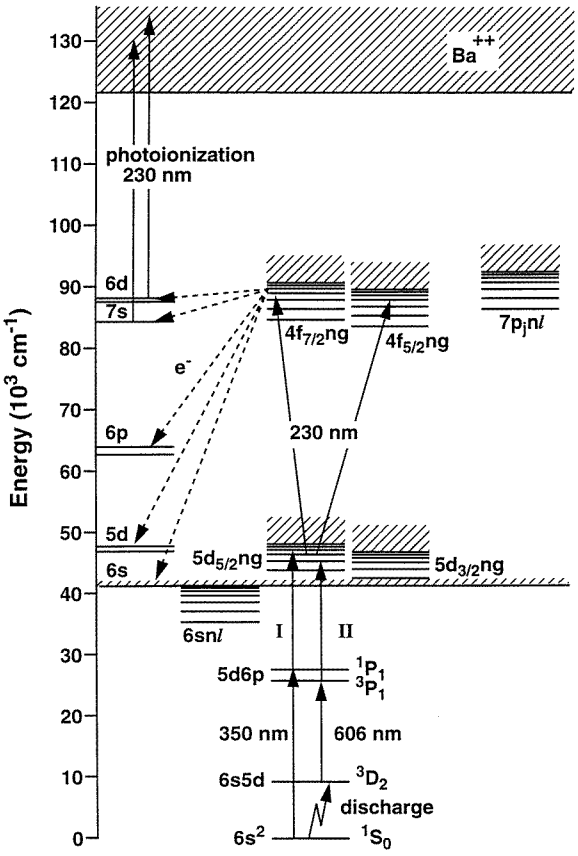

Figure 1. Energy level diagram and excitation scheme of 4fng autoionizing states of barium. The intermediate $5d_{5/2}ng[K]$ levels are populated in a two-step excitation either from the ground state via the 5d6p $^1P_1$ level (path I), or from the metastable 6s5d $^3D_2$ level via the 5d6p $^3P_1$ level (path II). The autoionization pathways of the 4fng levels are indicated by broken arrows. The photon energy of the pulsed dye laser driving the 5dng $\rightarrow$ 4fng transitions is sufficient to photoionize highly-excited Ba^+ $7s_{1/2}$, $6d_j$ and $4f_{5/2}$ ions produced in the autoionization process of 4fng states.

the slow electrons produced by the autoionizing 4fng states. Therefore we relied on the detection of Ba^{++} ions. As a consequence the atoms autoionizing in $6s\epsilon\ell$, $5d_j\epsilon\ell$ and $6p_j\epsilon\ell$ continua could not be observed.

To optimize the Ba^{++} signal the three dye laser pulses were spatially and temporally overlapped in the interaction region. In view of the long lifetimes of the intermediate 5d6p and 5dng states, the overlap in time of the dye laser pulses was not very critical. The interaction region was located 15 cm downstream from the oven between two capacitor plates (1 cm apart). During the laser excitation process the capacitor plates were held at zero potential to ensure field-free excitation of the Ba atoms. After a time delay of 0.5 μs a pulse of 300 V was applied to one of the plates sweeping the ions through a grid in the plate onto an electron multiplier tube. A grid at negative DC voltage, positioned in between the capacitor plate and the electron multiplier tube, was used to narrow down the temporal distribution of the ion signals. This facilitated the separation of the Ba^{++} signal from the

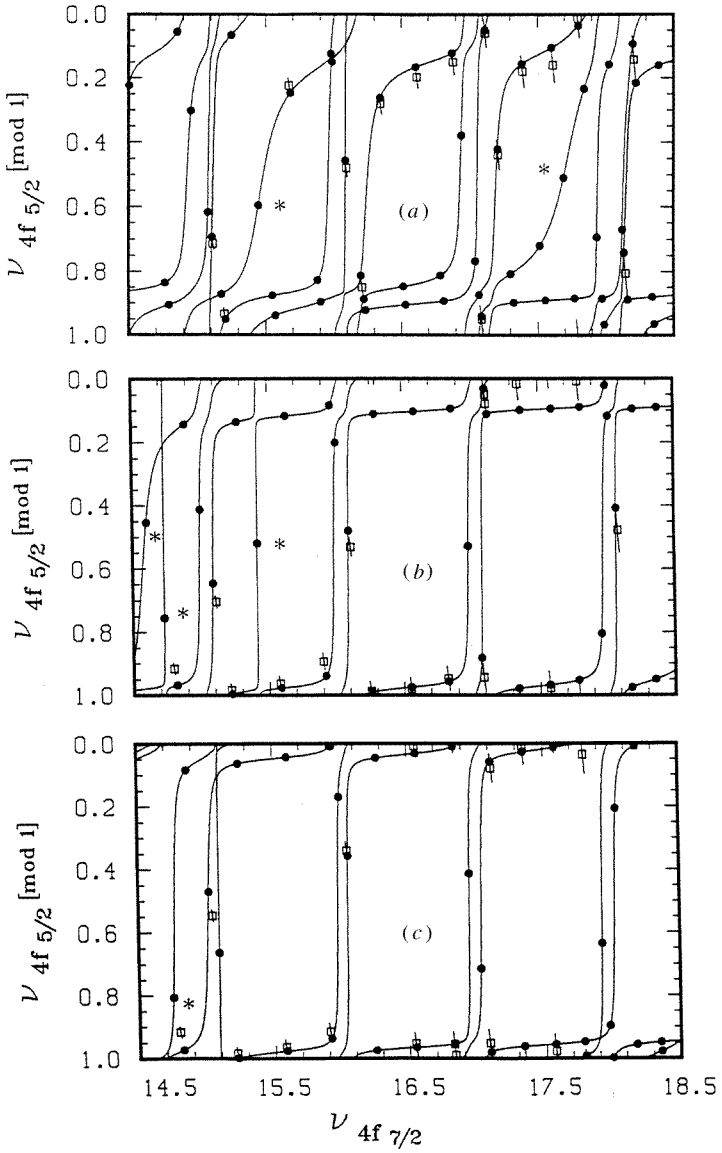

Figure 2. Lu–Fano plots in the energy range 90 000–90 200 cm^{-1} containing calculated (full circles on the theoretical curves) and experimental data points (open squares with error bars of $\pm 0.5\ cm^{-1}$). All closed channels (11) are included for $J' = 1$ (*a*) whereas the Lu–Fano plots for $J' = 2$ (*b*) and $J' = 3$ (*c*) are restricted to $4f_j ng_{j'}$ and $7p_j ns$, $d_{j'}$ channels only. The $7p_j ns$ and $7p_j nd_{j'}$ levels, classified in *jj* coupling, are denoted by an asterisk: (*a*) $7p_{3/2}12s$ ($\nu_{4f_{7/2}} \sim 15.5$) and $7p_{1/2}14s$ ($\nu_{4f_{7/2}} \sim 17.5$); (*b*) $7p_{1/2}12d_{5/2}$, $7p_{1/2}12d_{3/2}$ and $7p_{3/2}12s$ levels (in order of increasing energy); (*c*) $7p_{1/2}12d_{5/2}$ level.

strong Ba^+ signal resulting from the autoionizing intermediate state, and from a Sr^+ signal arising from impurities in the Ba sample.

The third dye laser was canned over the $5dng \rightarrow 4fn'g$ transitions in steps equal

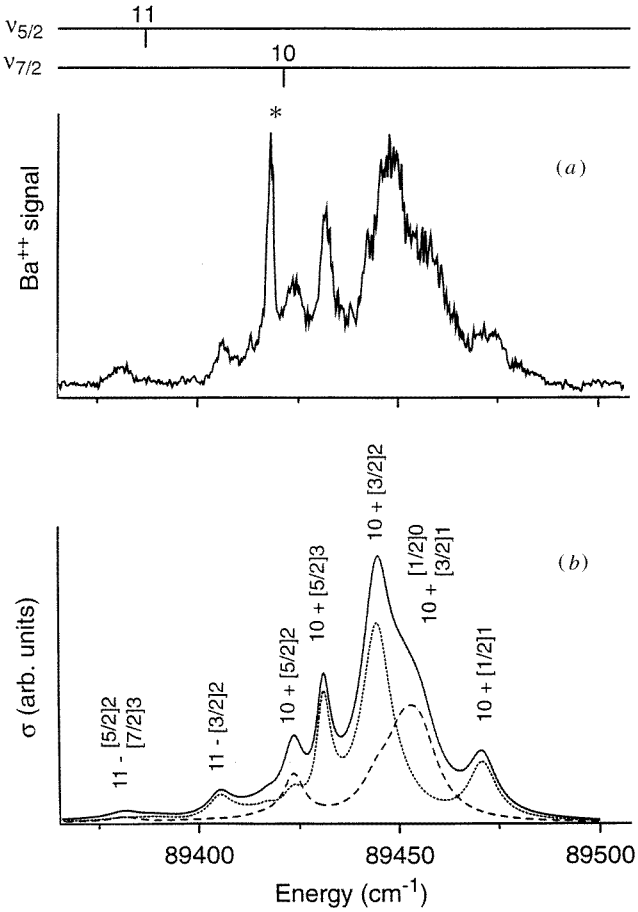

Figure 3. 4fng spectrum excited from the $5d_{5/2}10g[3/2]J$ level. The intermediate level is excited via path II. The energy scale is relative to the $6s^2$ ground state. (*a*) Experimental spectrum showing the recorded Ba^{++} signal versus energy. The Ba^+ $5d_{5/2} \rightarrow 4f_{7/2}$ transition is indicated by an asterisk. (*b*) Calculated spectra using the *R*-matrix method with assignments of the most prominent $4f_j ng$ resonances given in $n \pm [K']J'$ notation; the (+) and (−) signs are shorthand notations for $4f_{7/2}$ and $4f_{5/2}$, respectively. The dotted curve shows the calculated spectrum of $4f_j ng$ levels excited from the $J = 2$ component of the $5d_{5/2}10g[3/2]$ doublet. The dashed line shows the calculated spectrum of $4f_j ng$ levels excited from the $J = 1$ component of the $5d_{5/2}10g[3/2]$ doublet. The total calculated excitation spectrum, shown as a full curve, is the sum of the broken curve and the dotted curve.

to the bandwidth of the UV laser light (≈ 0.15 cm^{-1}). At each wavelength setting the integrated Ba^{++} signal of 12 laser shots was collected and stored on a computer. Although low power is required for the $5dng \rightarrow 4fn'g$ transitions, energies of ≈ 1 mJ per pulse were needed to subsequently photoionize the Ba^+ ions formed in the autoionization process of the 4fng levels. As a result several of the experimental spectra may show saturation effects. Examples of recorded spectra of 4fng states in energy ranges below the $4f_{5/2}$ threshold are shown in figures 3(*a*)–7(*a*), 9(*a*) and 10(*a*). These spectra will be discussed in section 3.2. Figures 3(*a*)–5(*a*) concern excitation spectra from the $5d_{5/2}10g[3/2]$ and $5d_{5/2}14g[K]$ intermediate levels, which were excited via path II from the metastable 6s5d

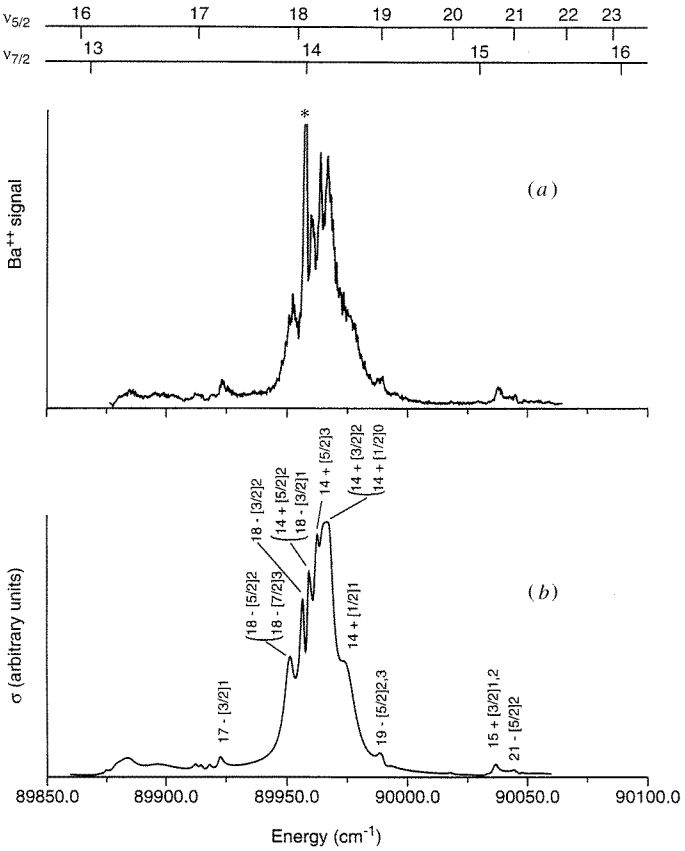

Figure 4. Spectrum of 4fng levels, excited from the $5d_{5/2}14g[3/2]$ $J = 1, 2$ level via path II. (*a*) Experimental spectrum showing the recorded Ba^{++} signal versus energy. (*b*) Calculated spectrum using the *R*-matrix method with assignments of the $4f_j ng$ levels in $n \pm [K]J'$ notation (see the text). Saturation in the experimental spectrum is accounted for using equation (1) with $N = 5$ to transform the calculated spectrum.

$^3D_2$ state. The recordings in figures 6(*a*), 7(*a*), 9(*a*) and 10(*a*) concern excitation spectra from $5d_{5/2}16g[K]$ and $5d_{5/2}17g[K]$ intermediate levels. Figure 11(*a*) shows an excitation spectrum of 4fng levels above the $4f_{5/2}$ ionization limit, also to be discussed in section 3.2. This 'shake up/down' $4f_{7/2}ng$ spectrum is obtained using the $5d_{5/2}26g[3/2]$ level as an intermediate level. The $n = 16$, $n = 17$ and $n = 26$ intermediate 5dng levels were excited from the ground state via path I.

3. Analysis and discussion

The observed spectra show a large variety in widths, profiles and quantum defects of the 4fng $J' = 0$–3 states, indicating strong channel interactions. The number of interacting channels in this energy range is too large to perform reliable empirical MQDT analyses of the spectra. We performed semi *ab initio* calculations based on the eigenchannel *R*-matrix method in combination with MQDT techniques (Aymar 1990, Greene and Aymar 1991) to

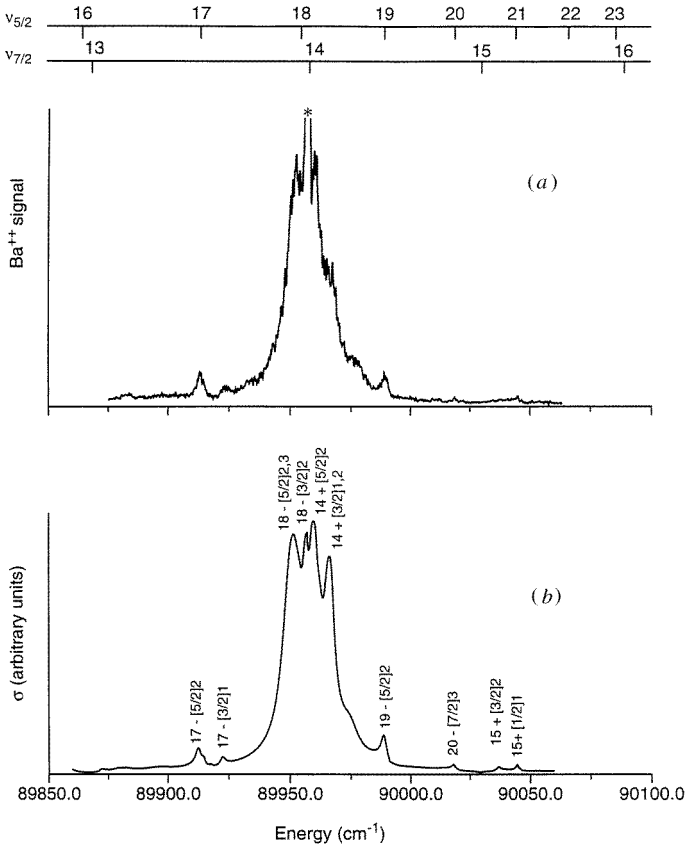

Figure 5. Same as figure 4 for the excitation spectrum from the $5d_{5/2}14g[5/2]$ $J = 2$ level.

analyse the complex spectra. The theoretical procedures used in the present work are the same as those used to describe the double circular 4f5g states (Aymar and Luc-Koenig 1995). For details we refer to the papers quoted above. *R*-matrix calculations were performed for odd-parity final states with $J' = 0$–3. For a given J' value the wavefunctions describing the valence electrons outside a frozen Ba^{++} core are determined variationally within a spherical reaction volume of radius $r_0 = 40$ au. Spin–orbit effects are explicitly taken into account within this reaction volume. The variational *R*-matrix calculation gives the logarithmic derivatives of the escaping electron's wavefunctions at the surface of the reaction volume which are then converted into a short-range reaction matrix. Using the short-range reaction matrix, the calculation of photoionization cross sections and the identification of resonances proceeds by standard MQDT techniques (Fano and Rau 1986).

To describe the odd parity $J' = 3$ final states $49n\ell jn'\ell' j'$ open or weakly closed channels, converging to Ba^+ 6s, $5d_j$, $6p_j$, 7s, $6d_j$, $4f_j$ and $7p_j$ thresholds, were included in the *R*-matrix calculations. For $J' = 2$ the number of included channels was 44, whereas for $J' = 1$ and $J' = 0$ this number was 32 and 12, respectively. The $J' = 1$, 2 and 3 symmetries include, respectively, 11, 16 and 19 closed channels attached to the $4f_j$ and $7p_j$ thresholds. The variational basis sets included up to 2100 two-electron functions. A large part of the variational basis functions represent various polarization and correlation effects

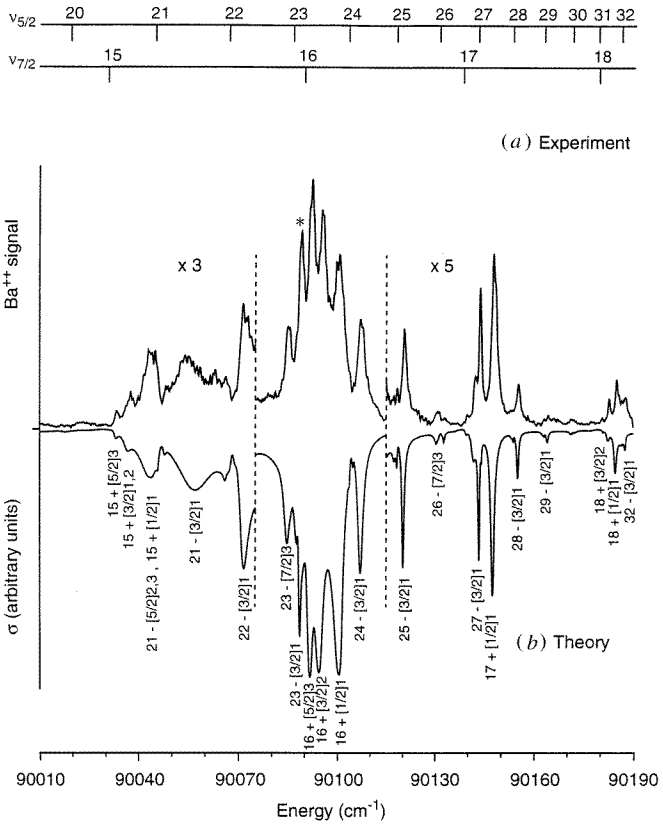

Figure 6. Comparison between experimental and calculated 4fng spectrum excited from the $5d_{5/2}16g[3/2]$ level. The intermediate 5dng level is excited from the ground state via path I. Saturation in the experimental spectrum is accounted for using equation (1) with $N = 5$ to transform the calculated spectrum. The wings of the ICE spectrum are blown up to show that the excellent agreement between experiment and theory extends towards the non-central energy region of the ICE spectrum. Excitation of the $4f_{5/2}23g[3/2]$ $J' = 1$ levels overlaps the ionic $5d_{5/2} \rightarrow 4f_{7/2}$ transition, denoted by an asterisk.

taking place within the reaction volume.

3.1. Channel mixing and identification of the resonances

As explained elsewhere (Fano and Rau 1986, Lecomte 1987), the complete short-range reaction matrix referring to closed and open channels can be contracted to give an effective reaction matrix restricted to closed channels only. Using this matrix, MQDT techniques adapted to bound spectra can be used to calculate the positions of resonant states (with an error comparable to their width), to analyse channel mixing by drawing Lu–Fano plots and to identify the levels. In figure 2 Lu–Fano plots in the energy range 90 000–90 200 cm^{-1}, are shown for (*a*) $J' = 1$, (*b*) $J' = 2$ and (*c*) $J' = 3$. All closed channels are included for $J' = 1$ (*a*). In contrast the Lu–Fano plots for $J' = 2$ (*b*) and $J' = 3$ (*c*) are restricted to $4f_j n g_{j'}$ and $7p_j n\ell$ channels only, i.e. 4f$n\ell$ with $\ell \neq 4$ were removed. Without this restriction, the Lu–Fano plots are unreadable. It is justified as the 4fng $J' = 2$ (or $J' = 3$) channels only weakly mix with 4fns, 4fnd and 4fni channels. Thus, the positions of 4fng$J' = 2, 3$

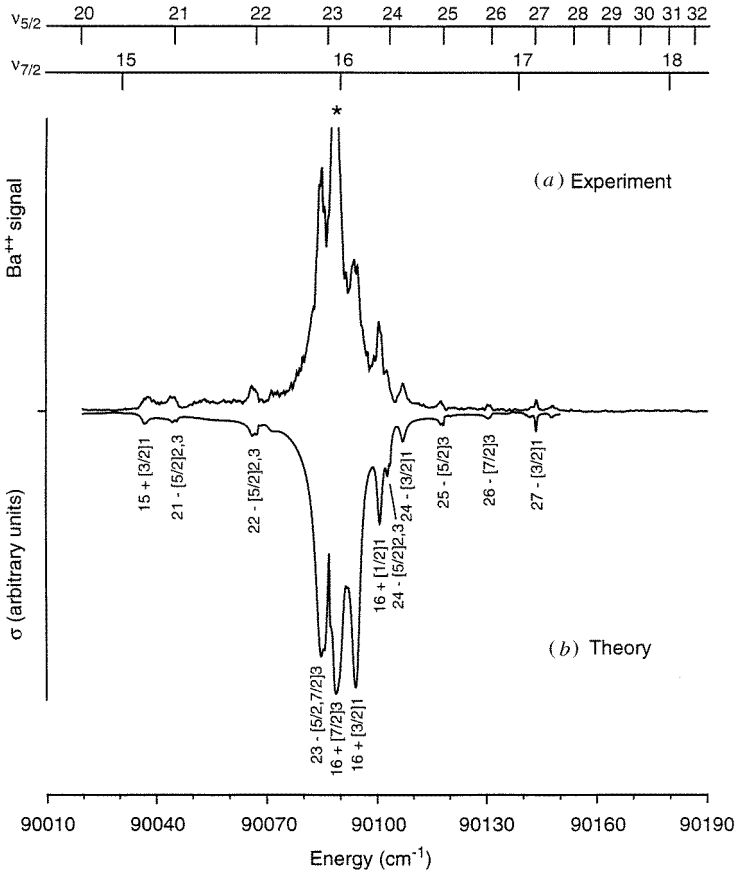

Figure 7. Same as figure 6 for the excitation spectrum from the $5d_{5/2}16g[5/2]$ $J = 2$ level.

levels are only slightly affected by removing those channels. For each J' value, the $7p_j ns$ and/or $7p_j nd$ perturbers are denoted by an asterisk. The gaps between the branches of the Lu–Fano plot give a visual estimate of the strength of the interaction between the $4f_{5/2}ng$ levels (lying on nearly 'horizontal' branches) and $4f_{7/2}ng$ and $7pn\ell$ levels (lying on nearly 'vertical' branches). For all J' symmetries, the dominant channel mixing is the $4f_{5/2}ng$–$4f_{7/2}ng$ channel mixing. This mixing is strongest for $J' = 1$. Figure 2 also shows that the perturbations of the $4f_{5/2}ng$ $J' = 1$ series by the $7p_{3/2}12s(\nu_{4f_{7/2}} \sim 15.5)$ and $7p_{1/2}14s(\nu_{4f_{7/2}} \sim 17.5)$ levels are stronger than the perturbations of $4f_{5/2}ng$ $J' = 2$ (or $J' = 3$) series by the $7p_{1/2}12d_j(\nu_{4f_{7/2}} \leqslant 14.8)$ and $7p_{3/2}12s(\nu_{4f_{7/2}} \leqslant 15.5)$; the branches of the Lu–Fano plots on which are lying the $7pns$ and $7pnd$ perturbers are less curved for $J' = 2$ or $J' = 3$ than for $J' = 1$. Test calculations performed with variational basis sets disregarding the $7p_j ns$ and $7p_j nd$ channels show that these channels are responsible for the strong $4f_{5/2}ng$–$4f_{7/2}ng$ $J' = 1$ channel mixing; indeed, by disregarding these channels, the perturbations of the $4f_{5/2}ng$ $J' = 1$ series are very localized, the quantum defect of $4f_{5/2}ng$ $J' = 1$ levels being almost n-independent. The influence of $7p_j ns$ and $7p_j nd$ channels on the energy level positions of $4fng$ $J' = 2$ (or $J' = 3$) levels was found to be less important than for

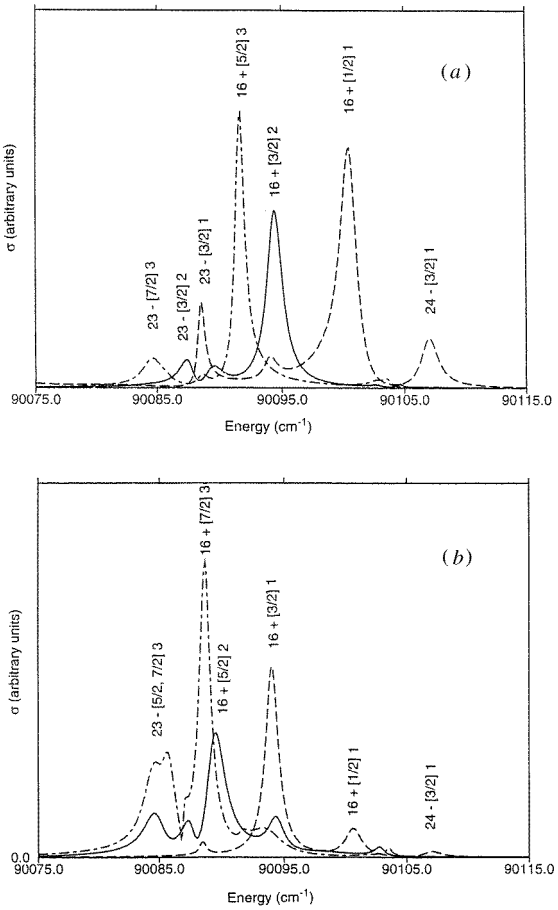

Figure 8. Contribution of the individual J' components of the calculated (unsaturated) 4fng spectrum corresponding to (*a*) the central region of figure 6(*b*) and (*b*) the central region of figure 7(*b*). The broken curve corresponds to $J' = 1$, the full curve to $J' = 2$ and the chain curve to $J' = 3$.

$J' = 1$. However, the large number of interacting channels makes it very difficult to specify the exact mechanisms responsible for the coupling between the 4fng and 7pns, d channels. Thus we have not attempted to determine more precisely the channel couplings responsible for the J'-dependence of the role played by the $7p_j ns$ and $7p_j nd$ channels.

The figures contain theoretical energy values as well as experimental values derived from several recordings (error bars of ± 0.5 cm^{-1}). For most of the levels, the theoretical energy falls within the experimental width of the resonance. Analysis of the decomposition of wavefunctions of each level on the complete set of closed channels allows the 4fng levels to be distinguished from 4f$n\ell$ ($\ell \neq 4$) and 7p$n\ell$ levels. It also gives the jK assignment of the 4fng resonances for a given J' value. Due to the mixing of 4fng levels with other closed channels and to the $4f_{5/2}ng$–$4f_{7/2}ng$ interaction, most of the resonances could not be identified with a purely 4fng jK-coupled level; the jK assignment corresponds to the dominant 4fng weight in the wavefunction expansion of each 4fng level. This dominant weight varies between 50% and 95% depending on the levels. Moreover, frequently reso-

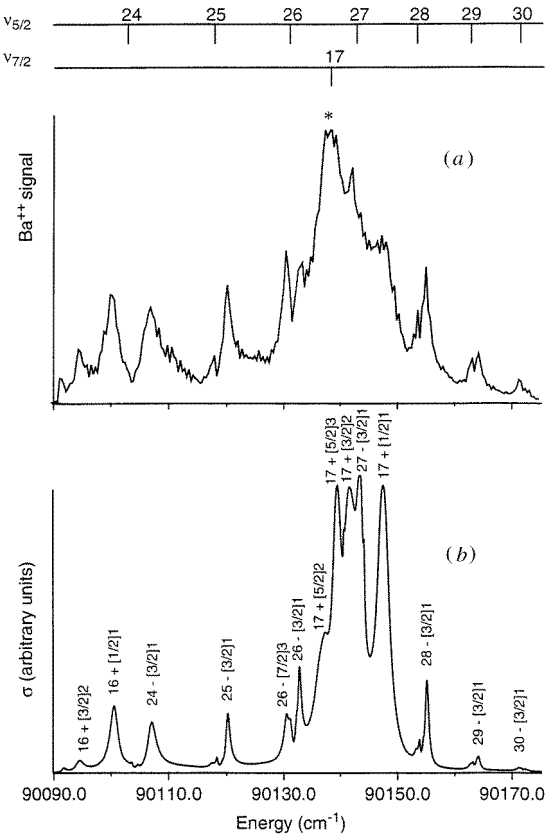

Figure 9. Comparison between experimental and calculated 4f*n*g spectrum excited from the $5d_{5/2}17g[3/2]$ level. The intermediate 5d*n*g level is excited from the ground state via path I. Saturation in the experimental spectrum is accounted for using equation (1) with $N = 7$ to transform the calculated spectrum.

nances corresponding to different J' values are almost degenerate. In this case assignments reported on figures 3–11 relate to those levels which contribute most to the resonance.

It should be noted that all observed resonances have a dominant 4f*n*g character in contrast with the resonances observed by Jones *et al* (1991) in their $5d_{5/2}5g[5/2]\ J = 2 \rightarrow 4f_j5g\ J' = 3$ ICE spectrum. In that case, in addition to the 4f5g resonances, some resonances could be ascribed to 6d*n*h levels (Aymar and Luc-Koenig 1995). Those resonances are only excited because of their strong mixing with the 4f5g levels. This emphasizes that correlation effects play a smaller role for high-lying 4f*n*g levels than for 4f5g levels. However, the significant role played by 7p*n*s d $J' = 1$ channels shows that correlation effects are far from being negligible for high-lying 4f*n*g levels.

3.2. Photoionization cross sections

The cross sections of the $5dngJ \rightarrow 4fngJ'$ photoionization process were calculated in the ICE approximation, which is based on negligible continuum excitation, excitation of the inner electron only, and absence of spatial overlap of the inner 5d or 4f electron and the outer *n*g

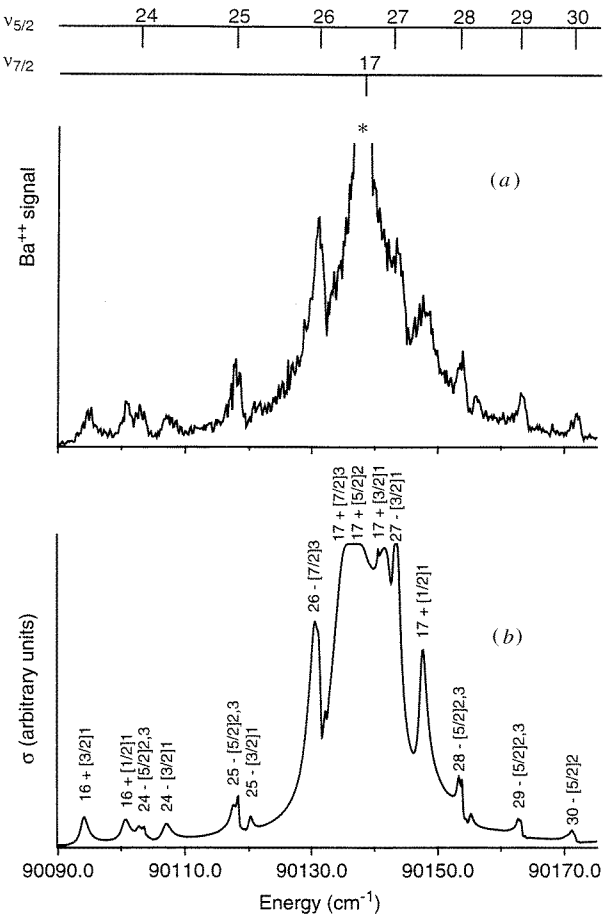

Figure 10. Same as figure 9 for the excitation spectrum from the $5d_{5/2}17g[5/2]$ $J = 2$ level. Saturation in the experimental spectrum is accounted for using equation (1) with $N = 10$ to transform the calculated spectrum.

electron. It was recently shown by Aymar and Luc-Koenig (1995) that the ICE approximation well describes the excitation of 4f5g levels from 5d5g levels. Excitation spectra of 4fng levels from $5d_{5/2}ng[5/2]$ $J = 2$, $5d_{5/2}ng[3/2]$ $J = 1$ and $5d_{5/2}ng[3/2]$ $J = 2$, were calculated assuming pure jK-coupling of the initial states. The validity of this assumption has been shown by Luc-Koenig *et al* (1995). From an initial 5dng $J = 2$ state, three $J' = 1$, four $J' = 2$ and four $J' = 3$ levels of the 4fng configuration can be reached, whereas from a 5dng $J = 1$ state also the $4f_{7/2}ng_{7/2}$ $J' = 0$ levels can be excited. The photoionization spectra are calculated on an energy mesh of 0.1 cm^{-1} which is comparable to the experimental width (≈ 0.15 cm^{-1}).

To compare experimental recordings with calculated spectra several features of the experiment have to be considered. First of all, since the 5dng $K = \frac{3}{2}$ doublet is unresolved in the experiment, both the $J = 1$ and the $J = 2$ component of the $K = \frac{3}{2}$ level were excited. The relative populations were estimated from phase-shifted MQDT parameters (Lecomte 1987) deduced from the calculations of 5dng excitation spectra by Luc-Koenig *et al* (1995).

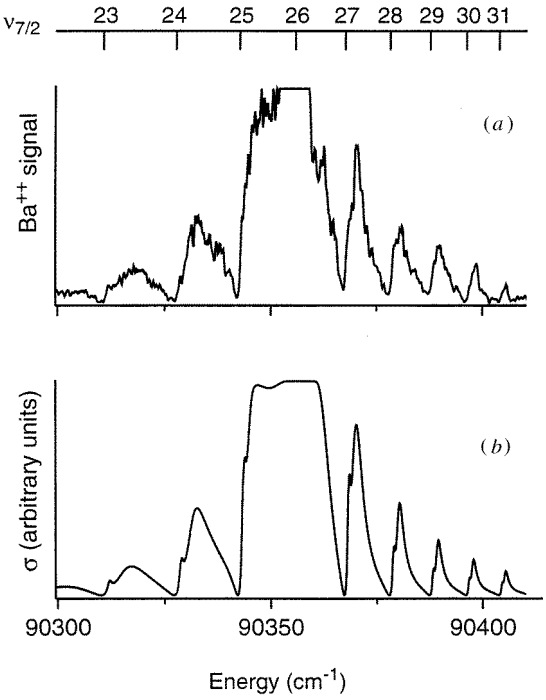

Figure 11. Excitation spectrum of $4f_{7/2}ng$ levels, located above the $4f_{5/2}$ ionization threshold at 90 293.49 cm^{-1}. Excitation of the intermediate $5d_{5/2}26g[3/2]$ levels took place via path I. (*a*) Experimental spectrum, the Ba^{++} signal resulting from ionic $5d_{5/2} \rightarrow 4f_{7/2} \rightarrow \epsilon\ell$ transitions is cut off to reveal more detail in the wings of the shake up/down spectrum. (*b*) *R*-matrix result with saturation parameter $N = 80$. The main broad peaks are members of the $4f_{7/2}ng[1/2]$ $J = 1$ Rydberg series.

The ratio of the cross sections for these transitions depends on the excitation path of the $5dng$ $K = \frac{3}{2}$ level. For excitation from 5d6p $^3P_1$ (path II) the ratio of the intensities of the $J = 1$ and $J = 2$ components of the $5d_{5/2}ng[3/2]$ doublet was found to be close to one for all n. In comparison between experimental and calculated spectra this ratio was therefore chosen equal to one. For excitation from 5d6p $^1P_1$ (path I) the intensity of the $J = 1$ level is three orders of magnitude smaller than that of the $J = 2$ level. This is not surprising since an unperturbed $5d_{5/2}ng[3/2]$ $J = 1$ level is a pure triplet state in an LS-coupling scheme. Population of the $5d_{5/2}ng[3/2]$ $J = 1$ level was therefore ignored in the calculations, when path I was used for excitation.

Secondly, due to the temporal overlap of the dye laser pulses involved in the excitation processes, angular coefficients related to the polarization of all three lasers have to be taken into account. The dye laser light is linearly polarized in the vertical plane, however in case of frequency doubling the polarization is rotated over 90°. As a result of crossed laser polarizations $\Delta M_J = \pm 1$ transitions are allowed. Although the effect of laser polarizations is largest when starting out from the $J = M = 0$ ground state it cannot be ignored for excitations starting out from 6s5d $^3D_2$ metastable level. Since the metastable levels are populated in a discharge we assumed that the population is evenly distributed over all possible M_J sublevels.

Thirdly, as the excitation spectra were recorded by detecting Ba^{++} ions produced

by photoionization of Ba^+ ions with UV light also used to drive the $5dng \rightarrow 4fng$ transitions, photoionization cross section of Ba^+ levels at the UV photon energy have to be calculated. This was done by using a central potential model approximation (Aymar *et al* 1984). Photoionization of 6d ions was found to be two orders of magnitude stronger than that of 7s ions and approximately equal to photoionization of $4f_{5/2}$ ions. Since photoionization of 7s ions is weak, experimental spectra are, below the $4f_{5/2}$ threshold, compared with partial photoionization cross sections of the $5d_{5/2}ng[K]J \rightarrow 4f_jn'gJ'$ processes corresponding to electron ejection into the $6d_j\epsilon\ell'$ continua only. Above the $4f_{5/2}$ threshold the experimental spectra are compared with the sum of the partial photoionization cross sections corresponding to autoionization into the $6d_j\epsilon\ell'$ and $4f_{5/2}\epsilon\ell'$ continua.

A fourth complication is related to the occurrence of saturation in the ICE transitions by the high UV power, required to produce Ba^{++}. To account for saturation effects in the recorded spectra the calculated spectra $\sigma(E)$ are transformed with the expression (Kachru *et al* 1985):

$$\sigma_N(E) = \sigma(E)(1 - e^{-N\sigma(E)/\sigma_m}) . \tag{1}$$

Here, σ_m is the maximum cross section and N is a saturation parameter to be adjusted to fit the experimental data. The total calculated spectrum consists of the weighted sum of spectra calculated for each possible J' symmetry following the procedures described above.

In figure 3 the eigenchannel R-matrix result (b) for the photoionization cross section from the $5d_{5/2}10g[3/2]$ doublet is compared with the recorded spectrum (a). The Ba^{++} signal resulting from the ionic $5d_{5/2} \rightarrow 4f_{7/2} \rightarrow \epsilon\ell$ transition is denoted by an asterisk. Since the $5d_{5/2}10g$ level was excited from 5d6p $^3P_1$, both $J = 1$ and $J = 2$ components were populated. The calculated $4fng$ spectrum excited from the $J = 2$ component of the $5d_{5/2}10g$ $K = \frac{3}{2}$ level is given by the dotted curve. The broken curve shows the $4fng$ excitation spectrum calculated from the $J = 1$ component. The total calculated excitation spectrum (full curve) is the sum of the broken and dotted curves. The total excitation spectrum reproduces the experiment much better than the individual spectra from either $J = 1$ or $J = 2$. This justifies the validity of the assumption of equal population of the initial $J = 1$ and $J = 2$ levels. Assignments of the most prominent resonances in the total excitation spectrum are given in $n \pm [K']J'$ notation (the $(+)$ and $(-)$ signs are shorthand notations for $4f_{7/2}$ and $4f_{5/2}$, respectively). In addition to $4f_{7/2}10g$ levels, which are directly accessible in the ICE process, $4f_{5/2}11g$ levels also appear in the spectrum. This is a result of the marked $4f_{5/2}ng$–$4f_{7/2}ng$ channel mixing. The calculated energy positions are within a few cm^{-1} of the experimental ones and their widths are also well reproduced.

In figures 4 and 5 the excitation spectra from the $5d_{5/2}14g[3/2]J$ and $5d_{5/2}14g[5/2]$ $J = 2$ intermediate state, respectively, are shown. The experimental spectra (figures 4(a) and 5(a)) are slightly saturated, this is accounted for in the calculations (figures 4(b) and 5(b)) by applying equation (1) with $N = 5$. Here again, channel mixing of $4f_jng$ series converging to different ionization thresholds is found to play an important role: $4f_{5/2}ng$ levels with $17 \leqslant n \leqslant 21$ appear. Moreover, $4f_{5/2}18g$ levels with $J' = 2$ and 3 appear in the spectrum from $5d_{5/2}14g[5/2]$ (figure 5(b)) with the same intensity as $4f_{7/2}14g$ levels. The intensities of the $4f_{5/2}18g[5/2]$ and $4f_{5/2}18g[3/2]$ $J' = 2$ resonances states are lower in excitation from $5d_{5/2}14g[3/2]$ than from $5d_{5/2}14g[5/2]$. Comparison of figures 4 and 5 shows that the calculation correctly reproduces the marked differences in the spectra recorded when exciting from initial levels with $K = \frac{3}{2}$ or $K = \frac{5}{2}$. The dependence of the cross section on the excitation path will be further documented below.

Figure 6 concerns the excitation spectrum from the $5d_{5/2}16g[3/2]$ level. As the $K = \frac{3}{2}$ level was excited from 5d6p $^1P_1$, only excitations from the $J = 2$ level were taken into

account in the calculations. Using $N = 5$ in equation (1) to account for saturation in the experimental recording a calculated spectrum (b) resulted which is in excellent agreement with the experimental spectrum (a). The wings of the ICE spectrum are blown up to show that the agreement between experiment and theory extends towards the non-central energy region of the ICE spectrum as well. The resonances, varying greatly in width, shape and intensity, could all be assigned. Many of them were identified as members of series converging to the lower $4f_{5/2}$ threshold. Most of the $4f_{5/2}ng$ levels are members of the $4f_{5/2}ng[3/2]$ $J' = 1$ series. This results from the fact that the $4f_{5/2}ng$–$4f_{7/2}ng$ channel mixing is strongest for $J' = 1$. In addition, the laser polarization scheme favours, in the experimental path (I), excitation of $J' = 1$ levels with respect to those with $J' = 2$ and 3. The experimental widths vary from 0.7 cm^{-1} at the high-energy side to ≈ 7 cm^{-1} at the low-energy side of the spectrum. Channel mixing results in variation with n of the resonance widths for the $4f_{5/2}ng[3/2]$ $J' = 1$ levels; in particular the large $7p_{3/2}n\ell$ component (~20%) in the wavefunction of the $4f_{5/2}21g[3/2]$ $J' = 1$ level is probably responsible for the large width for this resonance. The ionic $5d_{5/2} \rightarrow 4f_{7/2}$ transition in figure 6(a), denoted by an asterisk, overlaps with the $4f_{5/2}23g[3/2]$ $J' = 1$ level.

In figure 7 a similar comparison between the experimental spectrum (a) recorded from the $5d_{5/2}16g[5/2]$ $J = 2$ level and the calculated spectrum (b) is presented. Here again, the spectrum calculated with $N = 5$ in equation (1) accurately reproduces the complicated experimental spectrum. A detailed comparison of figures 6(a) and 7(a) shows that the observed spectra depend on the initial level from which the autoionizing resonances are excited.

Figure 8 shows the contributions of the individual J' components to the total calculated (unsaturated) $4fng$ spectra corresponding to the central regions of figures 6(b) and 7(b). The broken curve corresponds to $J' = 1$, the full curve to $J' = 2$ and the chain curve to the $J' = 3$ excitation spectrum. The structures on both sides of the intense peaks ascribed to $4f_{7/2}16g[K']$ levels correspond to $4f_{5/2}23g[K']$ and $4f_{5/2}24g[K']$ levels. It can be shown that from the $5d_{5/2}16g[3/2]$ $J = 2$ level, $4f_{7/2}16g[K']$ levels with $K' = J' - \frac{1}{2}$ are predominantly excited while from the $5d_{5/2}16g[5/2]$ $J = 2$ level, the excitation of $4f_{7/2}16g[K']$ levels with $K' = J' + \frac{1}{2}$ is favoured. These propensity rules agree with those obtained by calculating the angular part of the dipole matrix elements between pure jK-coupled $5d_{5/2}ng$ and $4f_{7/2}ng$ levels. In contrast, no simple propensity rule governs the excitation of $4f_{5/2}ng[K']J'$ levels which appear in the spectra owing to their mixing with the $4f_{7/2}16g[K']$ levels only. Comparison of figures 6(b) and 7(b) shows that only a few of the $4f_{5/2}ng$ levels with $J' = 1$ are excited from the $5d_{5/2}16g[5/2]$ level whereas many J' levels appear in the spectrum from $5d_{5/2}16g[3/2]$.

In figures 9 and 10 the experimental (a) and theoretical (b) excitation spectra from the $5d_{5/2}17g[3/2]$ and the $5d_{5/2}17g[5/2]$ initial levels, are displayed respectively. The saturation parameter used to calculate the spectra of figures 9(b) and 10(b) are, respectively, $N = 7$ and 10. Although the agreement between experiment and theory is not as good as in the spectra excited from the $5d_{5/2}16g[K]$ levels, the calculation well reproduces most of the experimental features. A discrepancy, however, concerns the description of the $4f_{7/2}17g[1/2]$ $J' = 1$ resonance: this resonance appears as a broad structure in figures 9(a) and 10(a) while it is a narrow and very intense resonance in the calculated spectra of figures 9(b) and 10(b). This resonance also shows up in the wing of the ICE spectrum from the $5d_{5/2}16g[3/2]$ level (see figure 6) and there it is perfectly reproduced by the calculation. The discrepancy is probably due to atomic beam density fluctuations during the measurements from $5d_{5/2}17g$ levels. Calculations account well for the differences in the autoionizing patterns for excitation from the $K = \frac{3}{2}$ and $K = \frac{5}{2}$ component of the

$5d_{5/2}17g$ $J = 2$ level. Most of the $4f_{5/2}ng$ levels appearing in the spectrum from the initial $K = \frac{3}{2}$ component correspond to $4f_{5/2}ng[3/2]$ $J' = 1$ levels, as also found for the excitation from $5d_{5/2}16g[3/2]$ (figure 6). In contrast, the spectrum from the $5d_{5/2}17g[5/2]$ shows many members of the almost degenerate $4f_{7/2}ng[5/2]$ $J' = 2$ and $J' = 3$ and Rydberg series. This illustrates the importance to use different initial levels to unravel complicated spectra involving degenerate resonances corresponding to different final J'-values.

Finally figure 11 compares the experimental and R-matrix result of the photoionization spectrum of $4fng$ levels excited from the intermediate $5d_{5/2}26g[3/2]$ $J = 2$ level. In the experimental spectrum (a), the ionic Ba^+ $5d_{5/2} \rightarrow 4f_{7/2}$ transition in the central region is cut off to reveal more detail in the wings of the spectrum. Since the energy interval lies above the $4f_{5/2}$ ionization threshold at 90 293.49 cm^{-1}, autoionization of the $4f_{7/2}ng$ levels also takes place into $4f_{5/2}$ continua. The spectrum shown in figure 11(b) is the sum of the partial photoionization spectra corresponding to electron ejection into the $6d_j\epsilon\ell'$ and $4f_{5/2}\epsilon\ell'$ continua. Both partial cross sections have the same order of magnitude. Saturation in the experimental shake up/down spectrum is simulated with a saturation parameter $N = 80$. The main broad peaks are identified as the members of the $4f_{7/2}ng[1/2]$ $J' = 1$ Rydberg series. The weak features visible in figure 11(b) are identified as $4f_{7/2}ng[3/2]$ $J' = 2$ and $4f_{7/2}ng[5/2]$ $J' = 3$ Rydberg levels which lie very close in energy. Here again, the prevalence of $J' = 1$ resonances results from the laser polarization scheme used in excitation path (I).

4. Concluding remarks

Autoionizing $4fng$ levels of barium, lying above the 6d threshold, have been studied both experimentally and theoretically. Series converging to the upper $4f_{7/2}$ and lower $4f_{5/2}$ thresholds were found to interact strongly. As a result of channel mixing the observed resonances vary widely in width, shape and intensity.

The purpose of the present paper is to show that recorded spectra in the energy range 6 eV above the first ionization limit in barium can be reproduced to a high level of accuracy in semi-*ab initio* R-matrix calculations in combination with MQDT. The actual information on the energy level structure and all detailed couplings of $4fng$ channels with perturber states and continua is contained in a short-range reaction matrix (the so-called K-matrix). Because this is a matrix calculated for each J symmetry, of size up to 49 and involving energy dependences, the information is too comprehensive to present in tables. However, the information is available upon request from one of the authors (MA).

The present information is of importance for the correct interpretation of excitation spectra of double Rydberg $Ngng$ states from $4fng$ states. Barium atoms in $Ngng$ states are of interest since both valence electrons then are in non-core penetrating orbits. In such states a helium-like three-body Coulomb system is approximated, which is ideal for studying electron correlation effects. $Ngng$ states are currently under investigation in our laboratory (Amsterdam).

Acknowledgments

We would like to thank Eliane Luc-Koenig for valuable discussions. Numerical calculations were carried out on the Cray 98 belonging to the 'Institut du Développement et des Ressources en Informatique Scientifique' of the Centre National de la Recherche Scientifique

and on the Cray YMPEL of the computer center ‘Paris Sud Informatique’.

References

Aymar M 1990 *J. Phys. B: At. Mol. Opt. Phys.* **23** 2697
Aymar M and Luc-Koenig E 1995 *J. Phys. B: At. Mol. Opt. Phys.* **28** 1211
Aymar M, Robaux O and Wane S 1984 *J. Phys. B: At. Mol. Phys.* **17** 993
Camus P, Gallagher T F, Lecomte J M, Pillet P and Pruvost L 1989 *Phys. Rev. Lett.* **62** 2365
Cooke W E and Gallagher T F 1978 *Phys. Rev. Lett.* **41** 1648
de Graaff R J, Ubachs W and Hogervorst W 1992 *Phys. Rev.* A **45** 166
Eichmann U, Lange V and Sandner W 1990 *Phys. Rev. Lett.* **64** 274
Fano U and Rau A R P 1986 *Atomic Collisions and Spectra* (New York: Academic)
Greene C H and Aymar M 1991 *Phys. Rev.* A **44** 1773
Jones R R and Gallagher T F 1990 *Phys. Rev.* A **42** 2655
Jones R R, Panming Fu and Gallagher T F 1991 *Phys. Rev.* A **44** 4260
Kachru R, van Linden van den Heuvel H B and Gallagher T F 1985 *Phys. Rev.* A **31** 700
Lecomte J M 1987 *J. Phys. B: At. Mol. Phys.* **20** 3645
Luc-Koenig E, Aymar M, van Leeuwen R, Ubachs W and Hogervorst W 1995 *Phys. Rev.* A **52** 208
Luc-Koenig E, Lecomte J M and Aymar M 1994 *J. Phys. B: At. Mol. Opt. Phys.* **27** 699
van Leeuwen R, Ubachs W and Hogervorst W 1994 *J. Phys. B: At. Mol. Opt. Phys.* **27** 3891
van Leeuwen R, Ubachs W, Hogervorst W, Aymar M and Luc-Koenig E 1995 *Phys. Rev.* A **52** 4567